Criticality and turbulence in a resistive magnetohydrodynamic current sheet

Alexander J. Klimas[1] and Vadim M. Uritsky[2]

[1]*University of Maryland, Baltimore County at NASA Goddard Space Flight Center, Greenbelt, Maryland 20771, USA*
[2]*Catholic University of America at NASA Goddard Space Flight Center, Greenbelt, Maryland 20771, USA*

Scaling properties of a two-dimensional (2d) plasma physical current-sheet simulation model involving a full set of magnetohydrodynamic (MHD) equations with current-dependent resistivity are investigated. The current sheet supports a spatial magnetic field reversal that is forced through loading of magnetic flux containing plasma at boundaries of the simulation domain. A balance is reached between loading and annihilation of the magnetic flux through reconnection at the current sheet; the transport of magnetic flux from boundaries to current sheet is realized in the form of spatiotemporal avalanches exhibiting power-law statistics of lifetimes and sizes. We identify this dynamics as self-organized criticality (SOC) by verifying an extended set of scaling laws related to both global and local properties of the current sheet (critical susceptibility, finite-size scaling of probability distributions, geometric exponents). The critical exponents obtained from this analysis suggest that the model operates in a slowly driven SOC state similar to the mean-field state of the directed stochastic sandpile model. We also investigate multiscale correlations in the velocity field and find them numerically indistinguishable from certain intermittent turbulence (IT) theories. The results provide clues on physical conditions for SOC behavior in a broad class of plasma systems with propagating instabilities, and suggest that SOC and IT may coexist in driven current sheets which occur ubiquitously in astrophysical and space plasmas.

I. INTRODUCTION

Historically, the exploration of self-organized criticality (SOC) [1,2] has been based on cellular automata such as sandpile and forest fire models. Although very instructive and convenient for theoretical analyses, these automata represent toy models rather than real-world physical SOC systems. In the meantime, a large body of observational evidence has been accumulated, indicating the existence of such systems in a broad range of settings (e.g., Refs. [3–9]). To understand critical dynamics in such systems, it is not enough to know basic universal principles controlling the SOC state—it is essential to describe how specifically these principles work in the particular physical environment.

In this paper, we investigate a plasma-physical model that exhibits robust critical dynamics described in terms of measurable plasma parameters coupled through a continuum system of resistive magnetohydrodynamic (MHD) equations. To simulate avalanche dynamics, we use the idea of modeling toppling events in a continuum diffusive system proposed by Lu [10] and adapt it for the case of current-driven magnetic diffusivity. We show the model possesses important hallmarks of SOC behavior such as critical scaling of susceptibility and finite-size scaling of avalanche statistics. At the same time, it exhibits signatures of intermittent turbulence in the velocity field satisfying the hierarchical model by She and Leveque [11]. We suggest that the coexistence between SOC and intermittent turbulence is a generic signature of continuum avalanching systems and predict its appearance in a large class of slowly driven active media.

Our current sheet model is motivated by Earth's magnetotail, which is the main driver for high-latitude geomagnetic activity revealing signatures of SOC dynamics [12]. The magnetotail is subject to loading of magnetic flux into its lobe regions, transport of the flux through its plasma sheet, and unloading in the earthward and tailward directions. Its global configuration includes a thin cross-tail current sheet [13] separating the reversed magnetic fields of the northern and southern lobes. The energy stored in the current sheet can be transported throughout anomalous resistivity regions created by localized kinetic instabilities [14] and removed from the system as a result of the reconnection process in the neutral plane of the current sheet [15].

II. THE CURRENT SHEET MODEL

We consider the current sheet to be the key structure responsible for avalanching transport and dissipation of magnetic free energy in the tail of a planetary magnetosphere. To model this process, we supplement the full set of two-dimensional (2d) resistive MHD equations with an evolution equation for magnetic diffusivity that is written in the form first introduced by Lu [10], who discussed a sandpile model based on a continuum diffusion equation with diffusion coefficient coupled to a field gradient equivalent to the local current density in the MHD fluid [16]:

$$\partial_t \rho + \nabla \cdot (\rho V) = 0, \tag{1}$$

$$\partial_t V + (V \cdot \nabla)V = -(4\pi\rho)^{-1}\nabla A(\Delta A) - \rho^{-1}\nabla P, \tag{2}$$

$$\partial_t A + (V \cdot \nabla)A = D\Delta A, \tag{3}$$

$$\partial_t P + V \cdot \nabla P + \gamma P(\nabla \cdot V) = (\gamma - 1)(4\pi)^{-1}D(\Delta A)^2, \tag{4}$$

$$Q = \ D_{\min}, |J| < \beta J_c \ \ D_{\max}, |J| > J_c, \tag{5}$$

$$\partial_t D = (Q(|J|) - D)/\tau. \tag{6}$$

The equations are written in dimensionless form. Parameters ρ, P, and V are respectively plasma density, pressure, and velocity; A is the y component of the vector potential

defining the magnetic field **B** in the studied 2d geometry; $J = -\Delta A/\sqrt{8\pi}$ is the scalar current density; $\gamma = 5/3$ is the adiabatic index; D is the diffusivity triggered by spatially distributed excitation parameter Q; and β is a numerical parameter explained below.

At any position, Q depends on the local current density and can take one of two values, D_{min} or D_{max}. The transition from D_{min} to D_{max} represents the excitation and saturation of a cross-field current-driven instability [17,18] when J exceeds a critical current density J_c; the reverse transition is a consequent quenching of the instability at a lower current density βJ_c, where $0 < \beta < 1$ is a numerical parameter controlling the width of the hysteresis loop. The instability evolves over kinetic time scales below the resolution of the MHD component, and so the Q transitions are assumed instantaneous. The diffusivity D follows these jumps in a continuous fashion with a characteristic delay time τ which is about 10^4 times longer than the simulation time step.

We solve the equations in the x-z plane under the assumption of zero spatial derivatives in the y direction. The model is driven by a steady, uniform inflow of plasma through the upper and lower boundaries at $z = \pm 1$ where we require $B_z \equiv \partial_x B_x \equiv 0$. One of perpendicular boundaries is closed and another one is open for the plasma. The initial and the driving conditions ensure that the field geometry is antisymmetric with respect to $z = 0$. We have obtained numerical solutions of the current sheet model on a 400×400 grid with $D_{min} \ll 1$ such that wherever $D = D_{min}$ the evolution is indistinguishable from ideal MHD over the observed time scales. A complete description of the simulation setup can be found in Ref. [16].

The inflowing plasma carries magnetic flux with it, consequently increasing the strength of the spatial field reversal and of its supporting current sheet. The current density inevitably reaches J_c at some position, thereby initiating an avalanche of magnetic flux toward the region near $z = 0$, where it is annihilated and converted to plasma kinetic and thermal energy [19,20]. This conversion process drives the plasma out of the simulation region through the open boundary. A small portion (10^{-3} to 10^{-2}) of the input magnetic energy is carried out through this boundary as well.

Eventually, the simulated plasma reaches a statistically stationary state in which the rates of magnetic energy and plasma mass flowing into the region are balanced, over long time scales, by the field annihilation rate and the outflow at the open boundary. After about 10^3 Alfven traversal times, this state takes the form shown in Fig. 1 of large scale global cycles made of long laminar periods during which plasma is loaded into the system but no active grid sites (with $Q = D_{max}$) are generated, followed by highly erratic unloading periods during which the magnetic field undergoes local transitions between frozen and unfrozen states analogous to stick-slip behavior of SOC models [21–24]. As shown in Fig. 1, energy dissipation occurs only during the unloading phases. Equal time snapshots of the magnetic field configuration, velocity field, and dissipation regions during an unloading time interval are shown in Fig. 2. Although the magnetic field appears smooth, the corresponding velocity field for the plasma is highly intermittent while at the same time well-defined regions of intense dissipation appear.
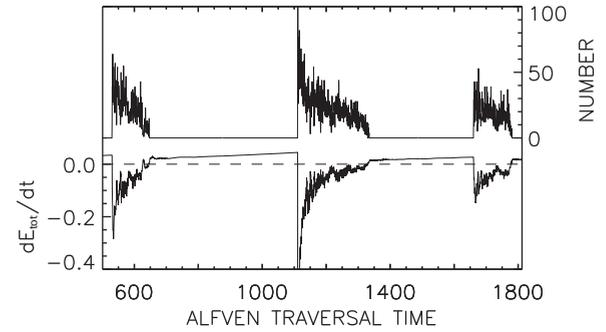

FIG. 1. Time series of the number of unstable grid sites with $Q = D_{max}$ through several cycles, and the corresponding time series of the total magnetic energy dissipation. Statistics shown in Figs. 4, 6 are obtained from the unloading cycles. Those separate quiet, laminar periods with no energy dissipation where the velocity field is smooth. Note that large-scale loading and unloading do not occur for cellular automata models, such as the BTW sandpile, or for many models of IT, but do happen, e.g., in magnetospheric dynamics [12].

A. Critical susceptibility

The global equilibrium conditions for a SOC state can be obtained in a mean-field approximation [25,26]. For sandpile models, these conditions have been formulated in terms of the probability h per unit time that a grid site will receive a grain of energy, the probability ϵ that a unit of energy will be dissipated by an unstable site, and the time-averaged fraction ρ_a of active sites. The infinite time-scale separation of standard sandpile models is recovered in the regime $h/\epsilon \to 0$ where the total
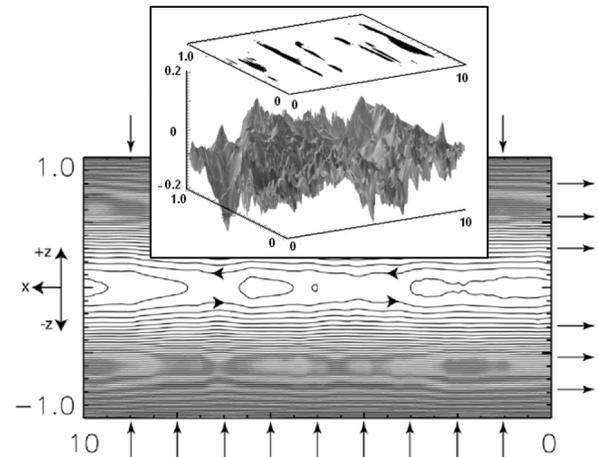

FIG. 2. Numerical simulation of a current sheet and its qualitative behavior (see Ref. [16] for details). The model is driven by a steady, uniform plasma inflow at the top and bottom boundaries as shown by arrows. The left boundary is closed, while the right is open. Plasma energized through annihilation in the spatial magnetic field reversal leaves the region at the right. Inset: (Top) A snapshot of regions where the diffusive Poynting flux (see text) exceeds a threshold, used to define avalanches. (Bottom) At the same time, the corresponding velocity field (v_x) in the system. Note that while the magnetic field lines appear smooth at this scale, the plasma velocity field is highly intermittent.

susceptibility of the system [26]

$$\chi_\epsilon = \partial \rho_a / \partial h|_{h=0} = 1/\epsilon \qquad (7)$$

diverges as $\epsilon \to 0$ and the SOC limit is approached. Central to obtaining this result is the existence of a steady state in which the average input energy flux is in equilibrium with the dissipated flux.

To identify such state in the current-sheet model, we have used Faraday's law to describe the equilibrium between magnetic flux inflow and dissipation through annihilation. Written in dimensionless variables [16], the x component of Faraday's equation in the given current sheet configuration with $\partial/\partial y \equiv 0$ reduces to $\partial B_x/\partial t = \partial E_y/\partial z$ for any x position. In the long-term limit, the dynamic equilibrium and the associated input-output balance of the electromagnetic energy are mainly controlled by the loading of oppositely directed magnetic fluxes at $z = \pm 1$ and their annihilation at $z = 0$. Below we express this condition in terms of the active site density ρ_a used in (7), thus obtaining the MHD equivalent of critical susceptibility in SOC sandpiles.

The dynamic equilibrium of the current sheet assumes that the time-averaged flux remains unchanged so that $\langle \int_0^1 B_z dx \rangle_t = $ const., or equivalently $\langle E_y(z=1) \rangle_t = \langle E_y(z=0) \rangle_t$. To the first approximation, the generalized Ohm's law for the electric field in the plasma frame yields $E_y = DJ_y - (\mathbf{V} \times \mathbf{B})_y = DJ_y - V_x B_z - V_z B_x$. Due to the applied boundary conditions, $V_x(z=1) = 0$, $V_z(z=1) = -V_b$, $B_x(z=1) = B_b$ (the subscript b denotes boundary values), and the current density $J(z=1)$ never reaches the critical level J_c so that $D(z=1) = D_{\min} \approx 0$. At $z = 0$, $B_x \equiv 0$ due to the antisymmetric field configuration, and the term $V_x B_z$ describing magnetic flux transport toward the open boundary is negligibly small compared to DJ.

Taking the above into account and averaging over x, we obtain the condition for the global steady state of the model

$$\langle V_b B_b \rangle_{x,t} = \langle D(z=0)J(z=0) \rangle_{x,t} \approx J_c \langle D(z=0) \rangle_{x,t}, \quad (8)$$

where we used a numerical result $J(z=0) \approx J_c$.

By applying the Laplace method, it is easy to show [27] that the formal initial-value solution to Eq. (6) is given by

$$D(t) = D(t=0)e^{-t/\tau} + \frac{1}{\tau} \int_0^t Q(s)e^{-(t-s)/\tau} ds, \quad (9)$$

which implies that $\langle D \rangle_t = \langle Q \rangle_t$ at any position, including $z = 0$, and therefore $\langle D(z=0) \rangle_{x,t} = \langle Q(z=0) \rangle_{x,t}$.

Finally, we define active grid sites in our model as those for which $Q = D_{\max}$ and introduce ρ_{af} for the time-averaged density of active grid sites. Assuming that the time average of $Q(z=0)$ is proportional to the total spatiotemporal average of this variable [27] and using the fact that $D_{\max} \gg D_{\min}$, we arrive at

$$\langle Q(z=0) \rangle_{x,t} = \xi \langle Q \rangle_{x,z,t} \simeq \xi \rho_{af} D_{\max}, \quad (10)$$

in which ξ is a numerical factor that is discussed below, and thus

$$\rho_{af} = \frac{\langle V_b B_b \rangle_{x,t}}{\xi J_c D_{\max}} = \frac{h_f}{\xi \epsilon_f}, \quad (11)$$

where h_f and ϵ_f are the averaged rates at which the magnetic flux is respectively added and dissipated.
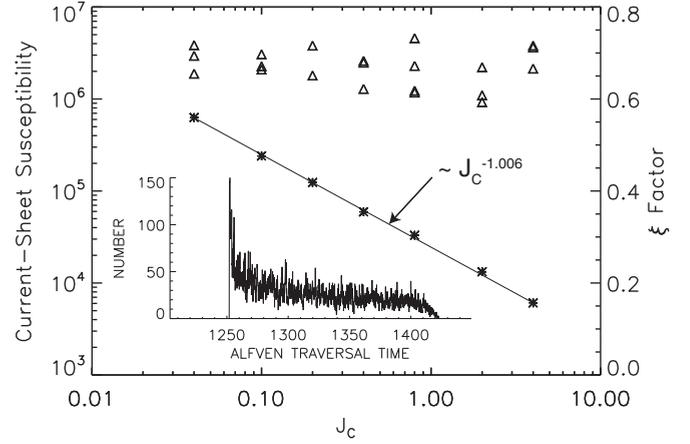

FIG. 3. For several J_c values ranging over a factor of 10^2, the quantity ξ (triangles, right axis) measured at different driving rates h_f, the susceptibility χ (stars, left axis), and the power-law fit to the susceptibility values providing the exponent γ. Inset shows an example of stochastic evolution of the number of unstable grid sites during a single global unloading.

Note that if $\xi \neq \xi(h_f, \epsilon_f)$, then $\partial \rho_{af}/\partial h_f \sim \epsilon_f^{-1}$, and the global susceptibility of the model diverges in accordance with the mean-field SOC behavior [26].

We have carried out a series of numerical simulations of the current-sheet model to examine the behavior of $\xi(h_f, \epsilon_f)$ with changes of both control parameters over approximately two orders of magnitude. Holding $D_{\max}$ fixed, ϵ_f was varied by varying J_c. For each of 7 chosen values of J_c, several runs for different h_f allowed for estimates of $\partial \rho_{af}/\partial h|_{h=0}$ through linear fits to $\rho_{af}(h)$, including the point $\rho_{af}(h=0) = 0$. Since SOC state implies clear time separation between driving and dissipation time scales, we required that h_f/ϵ_f was sufficiently small so that the behavior of the model consisted of active periods of fast dissipation separated by quiet periods during which slow magnetic flux inflow gradually refills the system.

Over the entire collection of simulation results satisfying this condition, no significant dependence of ξ on either h_f or ϵ_f has been found, and the total susceptibility followed the mean-field SOC scaling $\chi_\epsilon \sim \epsilon_f^{-\gamma}$ with $\gamma \approx 1$ (Fig. 3).

B. Energy avalanches

The critical divergence of current sheet susceptibility is supported by complex and violent unloading events (see inset in Fig. 3) which involve multiple avalanches of magnetic energy dissipation associated with propagating unstable regions.

Neglecting the convective contribution, the magnetic energy transported when a site becomes active is given by the magnitude $S_d(x,z) = (c/4\pi)\eta|\mathbf{J} \times \mathbf{B}|$ of the local diffusive Poynting flux [16], in which $\eta = 2\pi D/c^2$ is the anomalous resistivity and c is the speed of light. To observe avalanches, we used an automated technique for detecting and tracing regions having grid sites with S_d above a certain threshold. In analogy with avalanches in 2d sandpiles, we treat the events as (2+1)-dimensional spatiotemporal objects. Avalanches were identified by applying a floating activity threshold $S_{th}(t) = \langle S_d \rangle + k\sigma$ adjusted to the average value $\langle S_d \rangle$ and the standard

deviation σ of the Poynting flux at every time step. The floating threshold allows improved statistics, considering the time variation during unloading cycles. The time evolution of avalanches was obtained by checking the intersections of spatial regions above $S_{th}(t)$ in consecutive pairs of $S_d(x,z)$ snapshots.

Each avalanche was characterized by its lifetime T and its total Poynting flux, E, obtained from the integration of S_d over its spatiotemporal domain—grid sites with $S_d(x,z,t) > S_{th}(t)$ taking part in the avalanche. The linear dimensions l_x and l_z of avalanches were estimated by determining standard deviations of the x and z coordinates over all the grid sites involved in each avalanche (equally weighted). In addition the geometric mean $l_{xz} \equiv (l_x l_z)^{1/2}$, as well as the total area s, representing the total number of distinct pixels involved in the avalanche, were estimated. The statistics reported here were obtained using $k = 3.0$ and have also been reproduced in the range $k = 1.5$–4.0.

The probability distribution for lengths, time, area, and energy of avalanches all obey scale-free statistics. The first group of critical exponents was estimated based on analyses of probability distributions $p(T, s_{max})$ and $p(E, s_{max})$ constructed from subsets with $s \leqslant s_{max}$, in which s_{max} is defined to be the maximum area (number of pixels) of events included in the subset used to make the histogram. The normalized probability distributions were studied using the scaling *ansatz*

$$p(X, s_{max}) = X^{-\tau_X} f_X(X/X_c), \quad X_c \sim s_{max}^{\lambda_X}, \quad (12)$$

where $X \in \{E, T\}$ and f_X are scaling functions that are approximately constant for $X < X_c$ and drop rapidly for $X > X_c$.

Assuming Eq. (12), we have plotted the distributions in the rescaled coordinates $(X/s_{max}^{\lambda_X}, p(X)X^{\tau_X})$ and identified the combination of τ_E, τ_T, λ_E, and λ_T exponents that provides the best data collapse (Fig. 4). The resulting values $\tau_E = 1.48 \pm 0.02$ and $\tau_T = 1.95 \pm 0.03$ coincide with those reported earlier in Ref. [16]. The exponents $\lambda_E = 1.47 \pm 0.03$ and $\lambda_T = 0.68 \pm 0.04$ are consistent with the regression analyses for the expected values of energy and lifetime for avalanches with a given avalanche size s, within statistical error. These values also preserve the scaling relation $\lambda_T(\tau_T - 1) = \lambda_E(\tau_E - 1)$.

The anisotropy of the model leads to different growth rates of avalanches in the x and z directions. Hence $\langle s \rangle_{l_x} \sim (l_x)^{d_x}$ and $\langle s \rangle_{l_z} \sim (l_z)^{d_z}$ with $d_x = 1.40 \pm 0.03$ and $d_z = 3.11 \pm 0.06$. The geometric mean l_{xz} is related to s through another scaling relation, $\langle s \rangle_{l_{xz}} \sim (l_{xz})^{d_{xz}}$, with $d_{xz} = 1.97 \pm 0.05$, indicating that avalanches are compact. The exponent values obtained are consistent with $d_x^{-1} + d_z^{-1} = 2d_{xz}^{-1}$. We also studied E and T as functions of l_x and l_z and found that $\langle E \rangle_{l_x} \sim l_x^{\mu_x}$, $\langle T \rangle_{l_x} \sim l_x^{\nu_x}$, $\langle E \rangle_{l_z} \sim l_z^{\mu_z}$, and $\langle T \rangle_{l_z} \sim l_z^{\nu_z}$ with scaling exponents $\mu_x = 1.87 \pm 0.04$, $\nu_x = 1.13 \pm 0.01$, $\mu_z = 3.50 \pm 0.04$, and $\nu_z = 1.97 \pm 0.06$ (see the insets in Fig. 4). The ratios μ_x/μ_z and ν_x/ν_z are close to d_x/d_z, as expected.

All these results indicate that with respect to bursts of energy dissipation above the background, the system operates at or near a SOC state. Based on the values of the distribution exponents τ_E and τ_T, one can conjecture that the model operates near the mean-field limit. This is not typical for nondirected SOC sandpiles whose upper critical dimension d_u is usually higher than 2. However, it is possible that
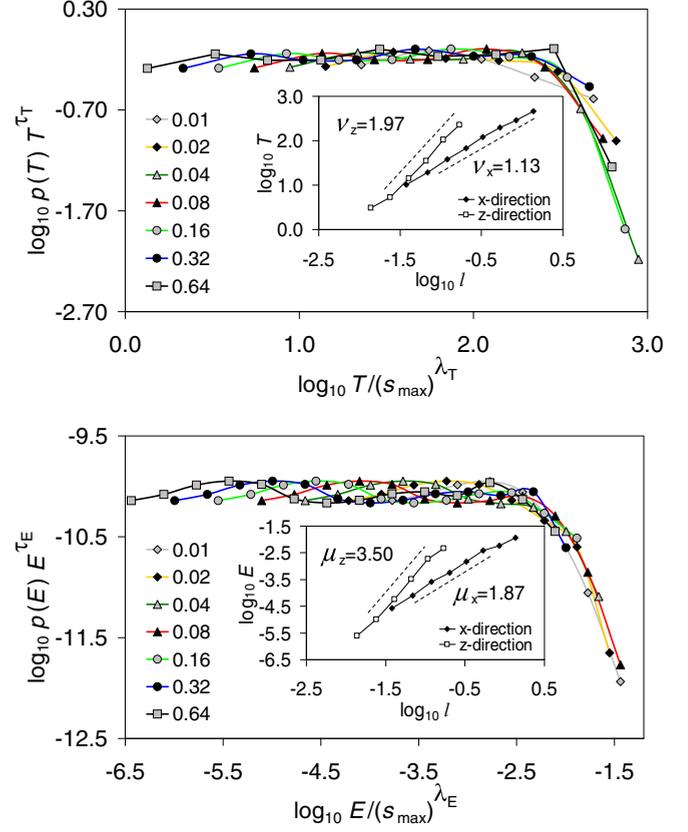

FIG. 4. Data collapse using Eq. (12) for avalanches with different maximum area s_{max} with $\tau_T = 1.95$, $\lambda_T = 0.68$, $\tau_E = 1.48$, and $\lambda_E = 1.47$. Insets: anisotropic scaling of E and T with the maximum avalanche extent l in x and z directions.

the avalanching dynamics in our model can be mapped onto the universality class of non-Abelian directed sandpiles with irreversible topplings [28], which exhibit the mean-field exponents starting from $d_u = 2$.

C. Velocity fluctuations

Energy avalanches in the model are accompanied by complex multiscale plasma flows. Figure 5 shows the initial expansion of a Poynting flux avalanche in back of an outward-propagating current wave as well as the associated transition from laminar to turbulent plasma flow at and in the interior of the expanding wave.

To analyze turbulence of the velocity field, we have followed the usual procedure by computing a set of equal time structure functions defined as $S_q(l) = \langle |\delta v_l|^q \rangle$, where $\delta v_l = [\boldsymbol{v}(\boldsymbol{r} + \boldsymbol{l}) - \boldsymbol{v}(\boldsymbol{r})] \cdot \boldsymbol{l}/l$ is the increment of the velocity $\boldsymbol{v}$ in the direction $\boldsymbol{l}$ (parallel to x or z axes), q is the order of the structure function, $l \equiv |\boldsymbol{l}|$ is the spatial displacement, and averaging indicated by $\langle \cdots \rangle$ is performed over all positions $\boldsymbol{r}$ and times during an unloading phase. For turbulent phenomena, $S_q(l) \sim l^{\zeta(q)}$ with $\zeta(q)$ defined by the turbulent regime under study. To extend the scaling range and improve the accuracy of this analysis, we have applied the method of extended self-similarity (ESS) [29] by plotting $S_q(l)$ versus $S_3(l)$.
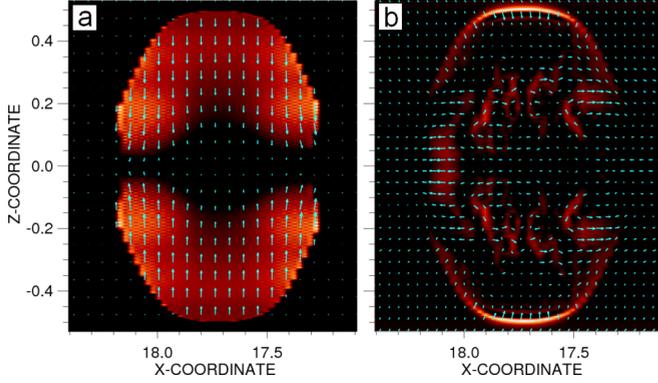
FIG. 5. The neighborhood of an initial site of instability shortly after the initiation of an unloading event. (a) Poynting flux due to slipping magnetic flux in the interior of the outward expanding current wave. (b) Transition from laminar to turbulent velocity field due to $\boldsymbol{J} \times \boldsymbol{B}$ acceleration at the current wave as it propagates through the magnetic field.

The resulting structure functions (Fig. 6) exhibit ESS over the entire range of scales available. The error bars shown are for $\zeta(q)/\zeta(3)$ in x direction; the errors in the z direction are about three times smaller. The values obtained in both directions are the same up to these errors. The dependence of $\zeta(q)/\zeta(3)$ on the order q shows a systematic departure from the Kolmogorov law $\zeta = q/3$, signaling intermittency. It can be fitted by the hierarchical model $\zeta(q) = (1 - \gamma)q/g + C[1 - (1 - \gamma/C)^{q/g}]$, in which C is the codimension of the most singular dissipative structures and g and γ are defined by $\delta z \sim \ell^{1/g}$ and $t_e \sim \ell^\gamma$, with t_e being the energy transfer time at the smallest inertial scales ℓ [30].

By choosing either $g = 4$, $\gamma = 1/2$, $C = 1$ (Iroshnikov-Kraichnan theory, IK, [31]) or $g = 3$, $\gamma = 2/3$, $C = 2$ (She and Leveque, SL, theory [11]) one can obtain rather accurate fits to the data. However, these results should be treated with

care because physical conditions for turbulence in our model are different from those in any of the listed hierarchical models. In the current sheet model, the intense current at leading energy avalanche fronts accelerates the fluid through the $\boldsymbol{j} \times \boldsymbol{B}$ force. These current structures play the role of energy sources rather than energy sinks (as would be the case in classical turbulence models). As we have shown in the previous section, the avalanches are scale free, and thus this driving mechanism appears at all scales as opposed to the standard picture of the direct turbulent cascade. To the best of our knowledge, at this point there is no IT theory that could predict the relationship between the magnetic energy avalanches and the intermittency in the velocity field (e.g., in the form of an exact law [32]), although it is evident that the resulting behavior is different from MHD turbulence [33].

III. CONCLUSION

Therefore, we have identified a slow driving rate regime in which the global susceptibility of the current sheet model diverges as the SOC limit is approached, in agreement with the mean field theory of SOC. The bursty transport of magnetic flux and energy into the field-reversal region of the current sheet exhibits scale-free avalanche statistics over broad ranges of scales. We have demonstrated the finite-size scaling of these statistics to confirm their intrinsic scale-free nature and revealed its intrinsic anisotropy, reflecting the geometrical configuration of the current sheet.

The results obtained suggest that the model operates in a slowly driven SOC state similar to the mean-field state of sandpile models. The geometric exponents in the direction parallel to the current sheet plane are close to the exponents of stochastic directed sandpiles above the upper critical dimension [28]. In the transverse direction, they are reminiscent of isotropic SOC models operating in the mean field such as the prototypical Bak-Tang-Wiesenfeld model [1].

Our simulation demonstrates that SOC behavior can be observed in a broad class of plasma models based on the full MHD system, plus our interpretation of the Lu [10] component in terms of a generic cross-field current-driven instability producing interconnected toppling events that can propagate throughout the system as avalanches. In particular, this mechanism can be responsible for the scale-free statistics of dissipation events in Earths's magnetotail, which are described by a similar set of exponents ($\tau_E = 1.5$, $\tau_T = 2.1$, $\lambda_E = 1.4$, $\lambda_T = 0.7$ [37–39]), as well as for a variety of other effects associated with intermittent turbulence in space plasma.

We found the spatial scaling of higher-order structure functions of the velocity field constructed using ESS to be in a formal agreement with some hierarchical models of turbulence, although no available IT model can adequately describe the simulated avalanching behavior. Our velocity analysis results point at an intricate connection between turbulent flows and energy avalanches that can play an important part in many classes of continuum systems with bursty dissipation [40–43], especially those involving reconnecting current sheets (see, e.g., Refs. [44–46]). The results obtained also reinforce a prior observation of coexisting signatures of SOC and IT in a single data set of ultraviolet images of the solar corona [33,47] and
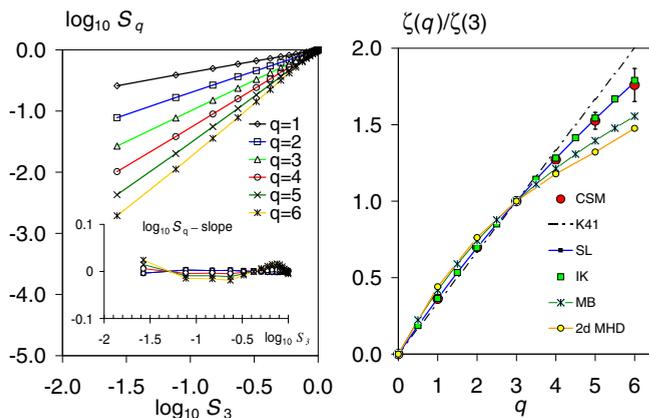

FIG. 6. Left: ESS plots of velocity structure functions with l parallel to the z axis. The inset shows the same functions with subtracted average slopes. Right: Dependence of $\zeta(q)/\zeta(3)$ on the order q for our current sheet model (CSM, with error bars), hierarchical models of IT mentioned in the text, Müller and Biskamp (MB) [34] model ($g = 3$, $\gamma = 2/3$, $C = 1$), Kolmogorov model (K41) [35], as well as the exponents from 2d ideal MHD simulations [36].

suggest that SOC and IT may be simultaneously measurable complementary phenomena in many astrophysical systems.

Finally, it is worth mentioning that temporal magnetic field reversals left outside the scope of our study can also lead to complex solutions. Temporal magnetic reversals play an important part in many natural systems, including the geodynamo and other planetary dynamos [48]. By breaking the symmetry of the flow, the magnetic field in such systems becomes oscillatory and can lead to a turbulent cascade described by universal scaling laws [48,49]. The von Karman sodium experiment (see, e.g., Refs. [50,51]) has demonstrated a variety of chaotic dynamo regimes when the flow forcing was not symmetric, including magnetic field reversals. In the future studies, it would be of interest to investigate critical turbulent properties of such dynamically reversed systems and to compare them with the spatial reversal dynamics explored here.

ACKNOWLEDGMENTS

[1] P. Bak, C. Tang, and K. Wiesenfeld, Phys. Rev. Lett. **59**, 381 (1987).

[2] P. Bak, C. Tang, and K. Wiesenfeld, Phys. Rev. A **38**, 364 (1988).

[3] V. I. Abramenko and V. B. Yurchyshyn, Astrophys. J. **597**, 1135 (2003).

[4] R. O. Dendy *et al.*, Phys. A (Amsterdam, Neth.) **340**, 607 (2004).

[5] G. Consolini and T. S. Chang, Space Sci. Rev. **95**, 309 (2001).

[6] D. L. Turcotte, Phys. Earth Planet. Inter. **111**, 275 (1999).

[7] J. P. Sethna *et al.*, Nature (London) **410**, 242 (2001).

[8] M. J. Aschwanden, N. B. Crosby, M. Dimitropoulou, M. K. Georgoulis, S. Hergarten, J. McAteer, A. V. Milovanov, S. Mineshige, L. Morales, N. Nishizuka *et al.*, Space Sci. Rev. **198**, 47 (2016).

[9] A. S. Sharma, M. J. Aschwanden, N. B. Crosby, A. J. Klimas, A. V. Milovanov, L. Morales, R. Sanchez, and V. Uritsky, Space Sci. Rev. **198**, 167 (2016).

[10] E. T. Lu, Phys. Rev. Lett. **74**, 2511 (1995).

[11] Z.-S. She and E. Leveque, Phys. Rev. Lett. **72**, 336 (1994).

[12] D. N. Baker *et al.*, J. Geophys. Res. [Space Phys.] **104**, 14601 (1999).

[13] A. Runov *et al.*, Ann. Geophys. **23**, 1391 (2005).

[14] J. P. Eastwood *et al.*, Geophys. Res. Lett. **32**, L11105 (2005).

[15] J. Birn *et al.*, J. Geophys. Res. [Space Phys.] **101**, 12939 (1996).

[16] A. J. Klimas *et al.*, J. Geophys. Res. [Space Phys.] **109**, 1426 (2004).

[17] A. T. Y. Lui, R. E. Lopez, S. M. Krimigis, R. W. McEntire, L. J. Zanetti, and T. A. Potemra, Geophys. Res. Lett. **15**, 721 (1988).

[18] A. T. Y. Lui, J. Geophys. Res. [Space Phys.] **101**, 13067 (1996).

[19] A. J. Klimas *et al.*, J. Geophys. Res. [Space Phys.] **105**, 18765 (2000).

[20] A. J. Klimas *et al.*, Geophys. Res. Lett. **32**, L14108 (2005).

[21] P. Bak and C. Tang, J. Geoph. Res.–Solid Earth Planets **94**, 15635 (1989).

[22] Z. Olami, H. J. S. Feder, and K. Christensen, Phys. Rev. Lett. **68**, 1244 (1992).

[23] M. Paczuski, S. Maslov, and P. Bak, Phys. Rev. E **53**, 414 (1996).

[24] M. Gedalin, M. Balikhin, D. Coca, G. Consolini, and R. A. Treumann, Phys. Rev. E **72**, 037103 (2005).

[25] C. Tang and P. Bak, J. Stat. Phys. **51**, 797 (1988).

[26] A. Vespignani and S. Zapperi, Phys. Rev. E **57**, 6345 (1998).

[27] V. M. Uritsky, A. J. Klimas, and D. Vassiliadis, Phys. Rev. E **65**, 046113 (2002).

[28] D. Hughes and M. Paczuski, Phys. Rev. Lett. **88**, 054302 (2002).

[29] R. Benzi, S. Ciliberto, R. Tripiccione, C. Baudet, F. Massaioli, and S. Succi, Phys. Rev. E **48**, R29 (1993).

[30] H. Politano and A. Pouquet, Phys. Rev. E **52**, 636 (1995).

[31] R. Grauer *et al.*, Phys. Lett. A **195**, 335 (1994).

[32] C. Connaughton, R. Rajesh, and C. Zaboronski, Phys. Rev. Lett. **98**, 080601 (2007).

[33] V. M. Uritsky, J. M. Davila, and S. I. Jones, Phys. Rev. Lett. **103**, 039502 (2009).

[34] W.-C. Müller and D. Biskamp, Phys. Rev. Lett. **84**, 475 (2000).

[35] A. Kolmogorov, Dokl. Akad. Nauk SSSR **31**, 538 (1941).

[36] H. Politano *et al.*, Europhys. Lett. **43**, 516 (1998).

[37] V. M. Uritsky *et al.*, J. Geophys. Res. [Space Phys.] **107**, A1426 (2002).

[38] V. M. Uritsky *et al.*, Geophys. Res. Lett. **30**, 1813 (2003).

[39] V. M. Uritsky *et al.*, Geophys. Res. Lett. **33**, L08102 (2006).

[40] P. Bak and M. Paczuski, Phys. A (Amsterdam, Neth.) **348**, 277 (2005).

[41] K. Chen and C. Jayaprakash, Phys. A (Amsterdam, Neth.) **340**, 566 (2004).

[42] K. R. Sreenivasan *et al.*, Phys. A (Amsterdam, Neth.) **340**, 574 (2004).

[43] M. Paczuski, S. Boettcher, and M. Baiesi, Phys. Rev. Lett. **95**, 181102 (2005).

[44] E. R. Priest and T. G. Forbes, *Magnetic Reconnection: MHD Theory and Applications* (Cambridge University Press, Cambridge, UK, 2000).

[45] M. J. Aschwanden, *Physics of the Solar Corona* (Springer, Berlin, 2005).

[46] S. C. Cowley *et al.*, Phys. Rep. **283**, 227 (1997).

[47] V. M. Uritsky, M. Paczuski, J. M. Davila, and S. I. Jones, Phys. Rev. Lett. **99**, 025001 (2007).

[48] U. R. Christensen, D. Schmitt, and M. Rempel, Space Sci. Rev. **144**, 105 (2009).

[49] C. J. P. Gissinger, Europhys. Lett. **87**, 39002 (2009).

[50] R. Monchaux, M. Berhanu, S. Aumaitre, A. Chiffaudel, F. Daviaud, B. Dubrulle, F. Ravelet, S. Fauve, N. Mordant, F. Petrelis *et al.*, Phys. Fluids **21**, 035108 (2009).

[51] J. Boisson, S. Aumaitre, N. Bonnefoy, M. Bourgoin, F. Daviaud, B. Dubrulle, P. Odier, J. F. Pinton, N. Plihon, and G. Verhille, New J. Phys. **14**, 013044 (2012).